Magnetic Resonance Imaging 102 (2023) 164–178

Contents lists available at ScienceDirect

Magnetic Resonance Imaging

journal homepage: www.elsevier.com/locate/mri

Evaluation of the efficacy of micro-Magnetic Resonance Imaging compared with light microscopy to investigate the anatomy of modern and ancient waterlogged wood

Valeria Stagno [a,b], Claudia Moricca [c,*], Laura Sadori [c], Emanuele Dell'Aglio [d], Rita Reale [e], Silvia Capuani [b]

[a] Department of Earth Sciences, Sapienza University of Rome, Piazzale Aldo Moro 5, 00185 Rome, Italy
[b] National Research Council—Institute for Complex Systems (CNR-ISC) c/o Department of Physics, Sapienza University of Rome, Piazzale Aldo Moro 5, 00185 Rome, Italy
[c] Department of Environmental Biology, Sapienza University of Rome, Piazzale Aldo Moro 5, 00185 Rome, Italy
[d] Department of Chemistry, Sapienza University of Rome, Piazzale Aldo Moro 5, 00185 Rome, Italy
[e] Chemistry Applied to Restoration, A. Galli Academy, Via Petrarca 9, 22100 Como, Italy

ARTICLE INFO

Keywords:
Magnetic resonance imaging
Light microscopy
Waterlogged wood
Archaeological waterlogged wood
Wood imaging

ABSTRACT

Light microscopy is the conventional method used to investigate wood anatomy, identify the wood taxon, and assess its conservation state. It generally requires the mechanical cut of thin sections from a sample to obtain informative images. When dealing with wooden artworks or ancient remains (*e.g.,* archaeological waterlogged wood), it is important to avoid sample destruction. In this work the efficacy of micro-magnetic resonance imaging (μ-MRI) to investigate the anatomy of waterlogged wood is assessed in comparison with light microscopy. Images along the three anatomical directions (transverse, tangential and radial) of six modern wood species and one archaeological specimen of waterlogged wood (from the Neolithic site "La Marmotta") were obtained both by μ-MRI and light microscopy. μ-MRI images were acquired virtually selecting 2D slices along the three wood anatomical directions. A 3D reconstruction was derived from 2D μ-MRI images. Conventional light microscopy histology was obtained by manually cutting thin sections. To the best of our knowledge, this is the first study in which high-resolution MR images and light microscopy images of the three anatomical directions of seven wood species are compared. The non-destructive μ-MRI approach allows to investigate the 2D and 3D topological organization of the whole waterlogged wood sample up to a resolution of 8 μm. Although the optical microscope attains higher image resolutions and remains superior in the observation of wood diagnostic characters, multiparametric μ-MRI provides physiological investigation complementary to light microscopy, giving information concerning both a single section and the whole volume of the sample. The presented study may represent a starting point for further improvements of μ-MRI techniques applied to the non-destructive investigation of waterlogged wood samples, especially those of interest for cultural heritage.

1. Introduction

Wood is a porous and fibrous structural tissue of trees and woody plants [1]. It contains a multitude of different types of cells, with several functions and geometry. Its porosity covers different dimensional scales, from nanometers to millimeters. Based on structural characteristics, two different groups of wood are recognized: softwoods (Conifers – cone-bearing seed plants) and hardwoods (Angiosperms – fruit bearing plants), characterized respectively by a more homogenous and a more heterogeneous wood structure. The distinct features of each taxon (*i.e.,* a group of one or more populations of organisms) are the basis for wood identification. They are also crucial to assess the conservation state of wooden remains [2–6]. The study of wood anatomy is a common practice in different disciplines, such as biology, palaeobotany, archaeology, conservation, restoration, engineering, and the timber industry (*e.g.,* Ghavidel et al. [7], Moricca et al. [8], Silva et al. [9]). The conventional way of doing this is by light microscopy. This methodology is classified as destructive, as it requires sampling a piece of wood and

* Corresponding author.
E-mail address: claudia.moricca@uniroma1.it (C. Moricca).

https://doi.org/10.1016/j.mri.2023.06.011
Received 8 February 2023; Received in revised form 4 May 2023; Accepted 17 June 2023
Available online 20 June 2023

cutting it. Wood has an approximately cylindrical structure, and its features are oriented in one of the three orthogonal directions. For this reason, it is necessary to cut thin sections along three anatomical planes: transverse, tangential, and radial. The transverse section (or cross-section) is oriented perpendicularly to the wood grain, whereas both the tangential and radial sections are oriented along the main axis of the wood grain [7,10]. The radial section is in the longitudinal-radial plane and is parallel to the rays, whereas the tangential section is found in the longitudinal-tangential plane and is tangent to the annual ring boundaries.

In the cultural heritage field, knowing the species of wood, its structural organization, and its conservation state allows one to understand its physical and chemical properties [11], extract information about past human activities, and plan future restoration interventions. Moreover, different wood anatomies and taxa characterize different climates, therefore the identification of ancient wood helps to reconstruct ancient ecosystems [12].

Specifically, when dealing with wooden artworks, because of ethical, aesthetic, structural, and commercial value issues, even collecting a sample can be complicated. The main limitation of light microscopy is related to the sample volume [9]. To reduce the impact on the artwork, only one sample with the smallest volume possible (usually a few millimeters) and in areas that would not affect the value of the object should be collected [13]. Moreover, it is preferable to limit sample destruction, allowing for it to be used for further analyses. In the specific case of archaeological waterlogged wood, *e.g.,* ancient shipwrecks [14,15], obtaining good informative images by conventional light microscopy, *i.e.,* by a manual cut of thin wood sections, may result tricky because of the spongy and fragile structure of the archaeological waterlogged wood caused by years of immersion in water. Some works [4,16,17] have pointed out the use of reflected light microscopy and confocal laser scanning microscopy as alternative tools to traditional light microscopy. Both these techniques do not require a thin section as they are based on the observation of the external surface of the wood fragment. They are therefore non-destructive and can be used to characterize wood *in-situ*. However, their application on archaeological waterlogged wood remains difficult as the water present within the sample and on its surface reflects light, making its observation much harder.

To overcome the limitations of hand-sectioning fragile ancient waterlogged wood, non-destructive and 3D imaging technologies have also been developed providing new insight into the spatial organization of wood and wood-water interactions [2,3,18–28]. Among these, proton Nuclear Magnetic Resonance (^{1}H NMR) is particularly suitable for the study of archaeological waterlogged wood. It is based on the study of the magnetic properties of hydrogen nuclei and on the resonance phenomenon. Resonance can be considered as an energy coupling that causes the ensemble of nuclei, when placed in a strong external static magnetic field, to selectively absorb, and later release, energy unique to those nuclei and their surrounding environment or lattice [29]. In this condition, an electric signal, called NMR signal is received by the RF probe as electromotive force. The NMR signal is proportional to the proton density and it decays exponentially in time because of spin-spin relaxation time processes quantified by the T_2 parameter [29]. Superimposing over the main static magnetic field, time-dependent and controlled magnetic field gradients, NMR images are obtained. Due to the spin-spin relaxation processes, to obtain images of sufficient quality, the sample investigated with NMR imaging (MRI) must be rich in liquid protons, *i.e.,* hydrogen nuclei characterized by a relaxation time longer than the time duration of the imaging acquisition sequences [30,31]. In this regard, wood is a material naturally rich in water (*i.e.,* hydrogen nuclei) confined and bounded at different degree to wood-structures showing a large range of T_2 values. The spin-spin relaxation is faster for water which strongly interacts with the wood polymers [32], less rapid in the case of cell walls bound water and much slower in the case of water that fills vessels and tracheids [28]. Therefore, when all the wood structures are filled with water, the different relaxation of water in the different structures provides the main contrast mechanism for observing the anatomy of the wooden tissues [2,3]. Moreover, because the NMR signal depends on several parameters, such as the relaxation times T_2 and T_2* and many other, it is also possible to perform a multiparametric investigation by acquiring MR images weighted on one of the above-mentioned parameters. Specifically, the transverse or spin-spin relaxation time T_2 is only affected by the spin-spin interactions, whereas T_2* takes into account both the spin-spin interactions and the field inhomogeneities [31,33]. In this way, by interpreting the T_2- or T_2*-weighted contrast in each point of the sample or in each pixel of the image, chemical-physical and physiological information about wood microstructure can be extracted. MRI is also a 3D imaging technique [27,34,35]. In fact, the possibility of acquiring images of the sample through the virtual selection of an infinite number of slices with an extremely variable orientation allows one to scan the entire volume of the sample and reconstruct its three-dimensional morphology.

This work aimed at evaluating the efficacy of micro-magnetic resonance imaging (μ-MRI) in investigating the anatomy of different modern and ancient waterlogged woods, and in detecting complementary information to those obtainable with traditional optical microscopy. To this end, a protocol based on the acquisition of a complete MRI virtual histology by various optimized MRI sequences was implemented. Moreover, the 3D reconstruction from 2D NMR images was presented. The MRI results were compared with those obtained from the traditional method of optical microscopy to point out its advantages and disadvantages. To the best of our knowledge, this is the first work in which high-resolution μ-MRI performed along the three anatomical planes of waterlogged wood has been compared to optical microscopy.

2. Materials and methods

2.1. Sample preparation

A total of seven wood samples were analysed in this work: six cylinder-like samples of about 1.5 cm in height and <1 cm in diameter belonging to different contemporary wood species and one archaeological waterlogged wood fragment of size 1 × 0.5 cm. The contemporary woods were identified as: *Picea abies* (L.) H. Karst. (spruce), *Pinus pinea* L. (stone pine), *Lovoa trichilioides* Harms (African walnut), *Entandrophragma cylindricum* (Sprague) Sprague (sapele mahogany), *Populus alba* L. (white poplar), and *Pouteria altissima* (A. Chev.) Baehni (tanganyika walnut). Their size was chosen to suit the NMR capillary tube of 10 mm in diameter and they were soaked in distilled water until they sank, which indicated their complete saturation, to increase the signal-to-noise ratio (SNR) and improve the MR image quality. The archaeological waterlogged wood sample was recovered from the Neolithic village “La Marmotta”, currently submerged by the waters of the Bracciano lake (Latium, Italy). It represents a fragment that had detached from a pole. The sample fragment was identified as *Fagus* cf. *sylvatica* [36] and it remained submerged for the last millennia. Due to its preservation by waterlogging, no sample preparation was required.

First, MR images of the three anatomical sections of wood, *i.e.,* transverse, tangential, and radial sections, were acquired by virtual sectioning of the seven wood samples. Then, thin sections in the transverse, tangential and radial direction of the wood fragments were mechanically cut to be observed and photographed through optical microscopy. Botanical nomenclature follows the World Flora Online [37]. Prior to this study, wood species were identified using the keys provided by Schweingruber 1990 [38] for European taxa (*P. abies*, *P. pinea*, *P. alba, Fagus* cf. *sylvatica*), and Wheeler 2011 [39] for the remaining species (*L. trichilioides*, *E. cylindricum*, *P. altissima*).

2.2. Magnetic resonance imaging

A Bruker Avance-400 spectrometer operating at 9.4 T with a 10 mm micro-imaging probe equipped with a high performance and high

strength magnetic field gradient unit characterized by a maximum gradient strength of 1200 mT/m and a rise time of 100 μs was used. T_2-weighted or T_2*-weighted images were obtained by a Multi Slice Multi Echo (MSME) or a Gradient Echo (GE) sequence, respectively, with parameters optimized for the different wood species and anatomical directions of wood. Both T_2-weighted and T_2*-weighted images were acquired on all the wood samples and among these the images that provided the best contrast were selected. Indeed, in the T_2-weighted images the contrast depends on water dynamics, whereas in the T_2*-weighted images the contrast is also affected by differences in the magnetic susceptibility between different wood tissues and it highlights more the paramagnetic impurities that may be present in wood. Table 1, Table 2 and Table 3 show the optimized parameters for the transverse, tangential and radial directions, respectively. The acquisition time necessary to perform MR images of the whole sample spanned from a minimum of 6 h when the lowest repetition time (TR), number of scans (NS) and matrix size (MTX) were selected, to a maximum of 36 h when the highest TR, NS, and MTX were selected. To maximize the NMR signal intensity in the MSME sequence, the TR was selected longer or at least equal to the specific T_1 of each wood sample, which was measured in our previous works [3,28]. The NS was chosen on the base of the signal intensity measured on the wood sample, which depends on how much water each wood species absorbs, on the type of wood and on the relaxation time T_2.

2.2.1. Multi-slice 2D acquisition for 3D reconstruction

T_2*-weighted images were also used to obtain a 3D reconstruction. For this purpose, 24 slices with thickness of 500 μm were selected along all the sample volume. The image matrix was 512 × 512, NS = 256, FOV = 0.7 × 0.7 cm^2, and TR = 1200 ms.

3D reconstruction from 2D MRI was obtained using the open-source image processing package Fiji (Fiji Is Just ImageJ) based on ImageJ2.

2.3. Optical microscopy

Thin sections of soaked wood were obtained manually using a razor blade following the anatomical directions of wood (transverse, tangential, and radial). They were mounted on specimen slides and covered by coverslips. The thin sections were observed using a Leica DM750 transmitted light microscope at different magnifications (40×, 100× and 200×). Pictures were acquired using a Leica ICC50 W transmitted light microscope integrated camera and the Leica Application Suite (version 4.13.0) software.

3. Results and discussions

This work aims at evaluating the efficacy of micro-magnetic resonance imaging (μ-MRI) in investigating different waterlogged wood anatomies, and to detect complementary information to those obtainable with traditional optical microscopy. To this end, in Figs. 1-7 the anatomical elements of seven different wood species, one of them archaeological, highlighted with MR imaging are here compared with those obtained with optical imaging. Each figure, from 1 to 7, is divided into three rows made of three images: in the first row the images display, respectively, the transverse (a), tangential (b) and radial (c) sections of the whole sample obtained by MRI; in the second row, a zoomed portion of the same NMR images is provided (d, e, and f) to better compare the MRI results with those of optical microscopy, focused on smaller portions of each sample; the third row shows the optical microscopy images obtained in the transverse (g), tangential (h) and radial (i) directions of wood. The macro- and micro-morphology of each wood sample investigated is described and discussed in the following sections.

3.1. Picea abies

In Fig. 1 the anatomy of *Picea abies* (spruce) is shown. All the MR images are T_2*-weighted, therefore their contrast depends on both T_2 and magnetic field inhomogeneities. Both MR and optical images show a homogeneous structure in the transverse section (Fig. 1a and d), typical of softwoods that are composed of one kind of repeated cells, *i.e.,* tracheids (conductor elements consisting of a single, elongated dead cell). Moreover, the weak variability in the grayscale contrast of the MR images indicates a gradual early−/latewood transition (white and light-blue arrow in Fig. 1a). Comparing the MR image of the transverse section with the one obtained using the optical microscope, it is possible to see the same features but with a different contrast. Fig. 1d and g show only one annual ring limit (red arrow), resin canals (tube-like structures surrounded by epithelial parenchyma cells which secrete resin; green arrow and red circle) and uniseriate rays (*i.e.,* made of only a single line of cells when observed tangentially; orange arrow). Conversely, the MR image of Fig. 1a highlights the presence of two annual ring limits, with each annual ring characterized by a gradual transition from earlywood to latewood. Here, many resin canals can be seen and most of them provide dark voxels in the MR images (red circle), which indicates that they are full of resin rather than water. This is also confirmed by optical microscopy in Fig. 1g. Nonetheless, some resin canals emptied and were soaked with water during the imbibition process. The cell wall thickness (pink arrow) visible in the optical image was not seen in the MR image both because of the lower resolution and the very short T_2 of bound water in the cell wall that produces a black contrast due to the already decayed NMR signal at the selected echo time (TE = 5 ms).

Fig. 1b shows the tangential section of the whole sample. Here, an area with incomplete water saturation (black contrast) is visible in the upper part of the sample. In the water-imbibed zone, the MR image displays the rays (orange arrow) and the tangential resin canals (green arrow). In the zoomed portion showed in Fig. 1e, it is possible to notice the uniseriate rays (orange arrow) and both full and empty tangential resin canals (red circles). Only one empty (*i.e.,* full of water instead of resin) tangential resin canal (red circle) can be observed in the optical image in Fig. 1h, along with several uniseriate rays (orange arrow). The ray cells that surround the resin canal can be observed both in the MR image and in the optical image. Fig. 1h confirms the anatomical features already observed with MRI but optical microscope, thanks to its higher resolution, also makes it possible to count the ray cells that, according to literature [38], have an average height of 10 to 15 cells per ray. Most of the rays observed through MRI and optical microscopy (Fig. 1e and h) appear to fall on the shorter side. Moreover, the optical microscopy image shows the presence of bordered pits (*i.e.,* cavities in the secondary

Table 1
Optimized parameters used to acquire the MR image of the transverse section of the seven wood species.

	P. abies	*P. pinea*	*P. alba*	*L. trichilioides*	*E. cylindricum*	*P. altissima*	*F. sylvatica*
Sequence name	GE	GE	MSME	GE	GE	GE	GE
Echo time/Repetition time (ms)	5/800	3/1200	6/1500	5/1000	4/1000	4/2000	2.7/800
Number of scans	100	128	128	64	128	128	256
Field of view (cm^2)	0.8 × 0.8	0.9 × 0.9	0.9 × 0.9	0.8 × 0.8	0.7 × 0.7	0.8 × 0.8	0.9 × 0.9
Matrix (pixels)	1024	512	512	512	512	512	512
Number of slices	4	4	2	2	2	3	10
Slice thickness (μm)	300	200	300	300	300	250	500
In plane-resolution ($μm^2$)	8 × 8	18 × 18	18 × 18	16 × 16	14 × 14	16 × 16	18 × 18

Table 2
Optimized parameters used to acquire the MR image of the tangential section of the seven wood species.

	P. abies	*P. pinea*	*P. alba*	*L. trichilioides*	*E. cylindricum*	*P. altissima*	*F. sylvatica*
Sequence name	GE	GE	GE	MSME	GE	GE	GE
Echo time/Repetition time (ms)	5/800	3/1200	5/800	6.6/2000	5/2000	4/2000	2.4/800
Number of scans	128	128	200	128	100	128	256
Field of view (cm^2)	1.0 × 1.0	1.4 × 1.4	0.9 × 0.9	0.8 × 0.8	0.9 × 0.9	0.9 × 0.9	1.5 × 1.5
Matrix (pixels)	1024	512	512	512	512	512	512
Number of slices	4	5	2	4	4	3	5
Slice thickness (μm)	250	200	150	250	250	250	500
In plane-resolution (μm^2)	10 × 10	27 × 27	18 × 18	16 × 16	18 × 18	18 × 18	29 × 29

Table 3
Optimized parameters used to acquire the MR image of the radial section of the seven wood species.

	P. abies	*P. pinea*	*P. alba*	*L. trichilioides*	*E. cylindricum*	*P. altissima*	*F. sylvatica*
Sequence name	GE	GE	GE	MSME	GE	GE	GE
Echo time/Repetition time (ms)	5/800	2.6/800	5/800	6.6/2000	5/2000	4/2000	2.4/800
Number of scans	128	64	200	128	100	128	256
Field of view (cm^2)	1.0 × 1.0	1.4 × 1.4	0.9 × 0.9	0.8 × 0.8	0.8 × 0.8	0.9 × 0.9	1.5 × 1.5
Matrix (pixels)	1024	512	512	512	512	512	512
Number of slices	4	4	2	4	4	5	5
Slice thickness (μm)	250	200	150	250	250	250	500
In plane-resolution (μm^2)	10 × 10	27 × 27	18 × 18	16 × 16	16 × 16	18 × 18	29 × 29

wall of a cell, together with their outer sealing membrane, covered by a dome) on the tracheids wall (light-blue circle).

To distinguish spruce from other softwood species the radial section is of fundamental importance, as it allows one to observe the number and type of pits in the cross-field (*i.e.,* pits in the rectangle formed in the radial section by the walls of a ray cell and those of an axial tracheid), which vary among different softwoods. MR images displayed in Fig. 1c and f are characterized by a resolution of 10 × 10 μm^2, which is insufficient to recognize pits and cross-fields. Therefore, the radial section obtained with MRI cannot provide useful information about the diagnostic characters of spruce. Here, it is only possible to see the longitudinal section of tracheids (blue arrow) and the shadow of rays (yellow arrow). In contrast, the optical image in Fig. 1i shows the presence of cross-fields with piceoid pits (cross-field pits with a tight, often slightly overflowing, opening; green circle). The ray tracheid walls can be described as smooth and wavy.

3.2. *Pinus pinea*

The anatomy of *Pinus pinea* (stone pine) wood is shown in Fig. 2. In Fig. 2a, many annual rings with an abrupt shift from earlywood (white arrow) to latewood (light-blue arrow) can be observed. The abrupt early−/latewood transition is suggested by the strong difference of contrast between the brighter earlywood area and the darker latewood area. This different contrast is due to the different dynamics of water stored in the tracheids of earlywood and latewood. Indeed, the water in the latewood tracheids, which have a smaller lumen, is more hindered and characterized by shorter T_2 values compared to the water stored in the earlywood tracheids, which have a larger lumen size. The green arrow in Fig. 2a shows one of the many full resin canals that are better visible in the zoomed MR image (Fig. 2d) and in the optical image (Fig. 2g). In contrast, the red circle in Fig. 2d and g indicate an empty resin canal. In particular in Fig. 2d, the resin canal of the latewood area is surrounded by a circle of thin-walled epithelial cells [38], characterized by lighter MRI image voxels, also observable in Fig. 2g. The red arrow and the orange arrow in Fig. 2d and g indicate, respectively, the annual ring limit and one ray. The cell wall thickness (pink arrow) observed through optical microscopy was not seen by MRI. This can be due to the lower MRI resolution and/or the very short T_2 of bound water in the cell wall that produces black image voxels due to the already decayed NMR signal at the selected echo time (TE = 3 ms).

The tangential section of the sample (Fig. 2b and h) shows the presence of tangential resin canals (green arrow) and rays (orange arrow). In particular, in Fig. 2e the presence of a tangential resin canal (green arrow) inside the ray is highlighted. This can be better seen in the optical image (green arrow). Both MRI and optical microscopy confirm that pine wood has uniseriate rays with an average height of 8–15 cells, in accordance with the literature [38].

As mentioned above for the case of spruce, the MR image of the radial section has a resolution which is insufficient to recognize pits and cross-fields, therefore only the shadow of rays (yellow arrow) and the longitudinal section of tracheids (blue arrow) are visible in Fig. 2f. Optical image in Fig. 2i, instead, shows cross-fields with 2 to 4 pits, mainly pinoid (green circle), and uniseriate tracheid pits (light-blue circle). The cell walls vary from wavy and smooth to dentate.

3.3. *Lovoa trichilioides*

Lovoa trichilioides (African walnut) is a hardwood, as clearly seen in Fig. 3, that shows a diffuse porosity with indistinct ring boundaries. The MR image of the transverse section in Fig. 3a is T_2*-weighted, whereas those of the tangential and radial sections in Fig. 3b and c are T_2-weighted. In Fig. 3d and g vessels (5–20 vessels per square millimeter) with a mean diameter of 100–200 μm are indicated using light-blue arrows, along with rays (orange arrows) and thin- to thick-walled fibres (white arrows). Axial parenchyma (*i.e.,* tissue composed of typically brick-shaped cells) was detected both on the optical image and MR image (pink arrows). It is confluent, vasicentric, aliform and scanty paratracheal, with each strand composed by four or eight cells. In Fig. 3d, it is possible to see that parenchyma cells are characterized by lighter image voxels than fibres. This suggests that the lumen of fibres contains water which is restricted in smaller spaces. For this reason, it is characterized by T_2 shorter than 5 ms. Conversely, axial parenchyma cells are characterized by water in larger spaces, showing T_2 longer than 5 ms. Therefore, even if we did not directly observe fibres lumen in the MR image, we can state that they have a smaller size than parenchyma cells.

The image of the tangential section obtained by MRI only allows to identify rays (orange arrow) and vessels (yellow arrow). It should be noticed that the gray tones of the image voxels associated with the rays are quite light indicating they are wide and characterized by water with T_2 longer than about 7 ms. The high-resolution image in Fig. 3h shows

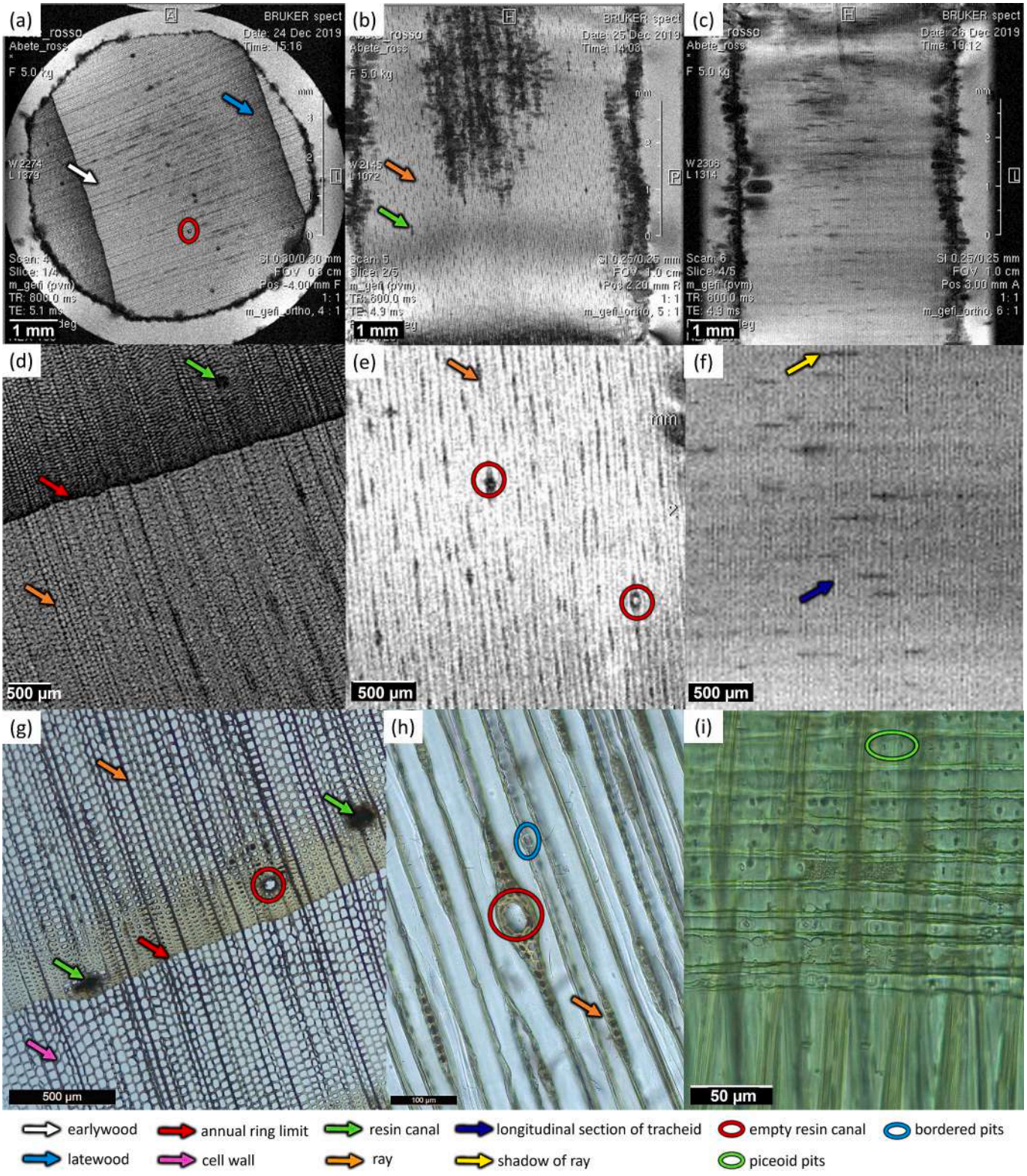

Fig. 1. Diagnostic features of *Picea abies* (spruce) wood investigated by the NMR virtual histology of (a) transverse, (b) tangential and (c) radial section with their zoomed portion (d-f) and the optical histology obtained by mechanical cut of (g) transverse, (h) tangential and (i) radial thin section.

large rays (most of which are 4-seriate, orange arrow) with gums and other deposits (green circle). Septate (blue arrow) fibres are present along with simple to minutely bordered pits (pink circle).

In Fig. 3f only vessels can be recognized (yellow arrow). The optical image in Fig. 3i allowed us to observe remarkably heterogeneous rays, with elongated and upright and/or square cells. Moreover, minute (< 4 µm) and alternate inter-vessel pits with polygonal shape (light-blue circle) and vessel-ray pits with distinct borders (red circle) can be identified.

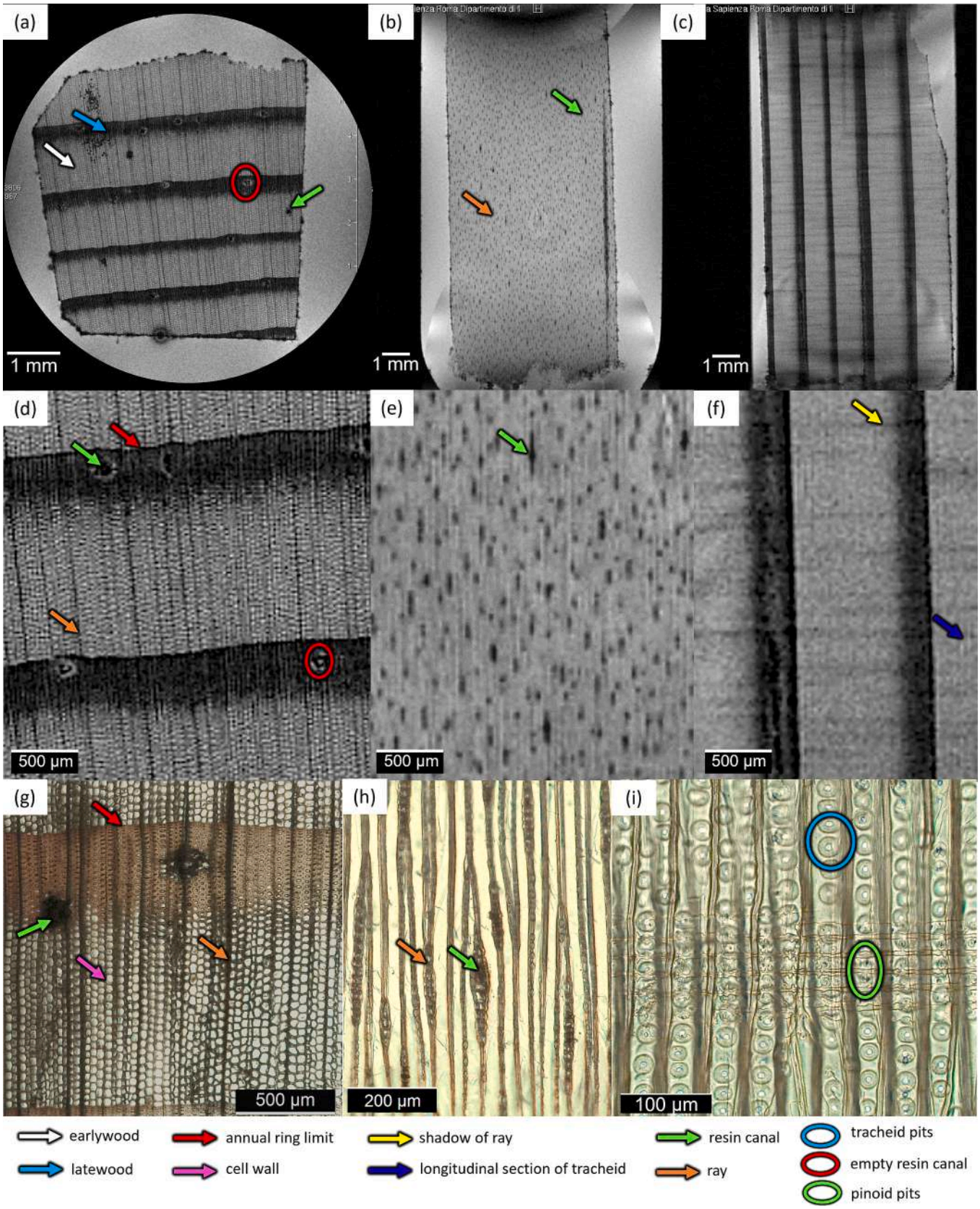

Fig. 2. Diagnostic features of *Pinus pinea* (stone pine) wood investigated by the NMR virtual histology of (a) transverse, (b) tangential and (c) radial section with their zoomed portion (d-f) and the optical histology obtained by mechanical cut of (g) transverse, (h) tangential and (i) radial thin section.

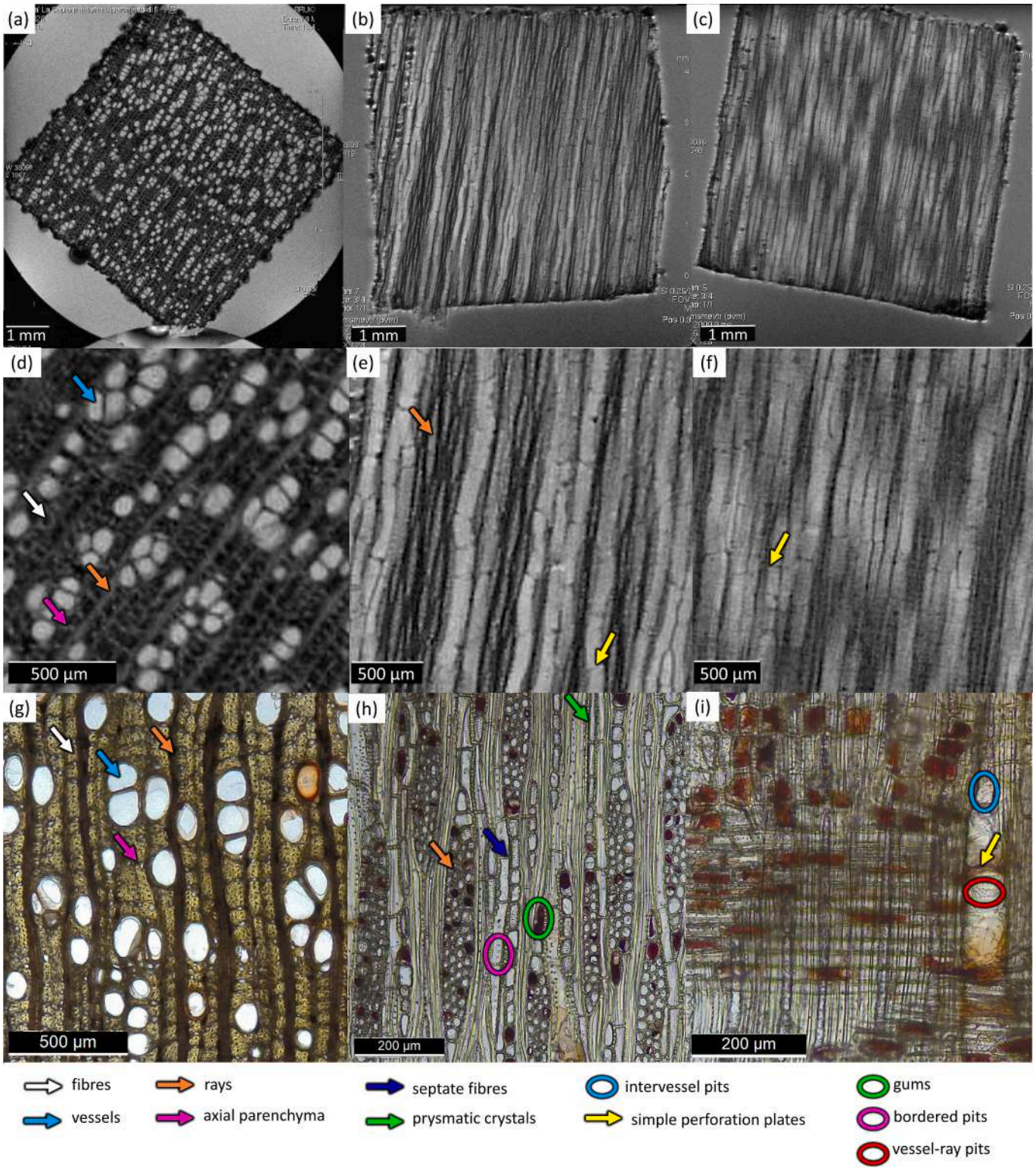

Fig. 3. Diagnostic features of *Lovoa trichilioides* (African walnut) wood investigated by the NMR virtual histology of (a) transverse, (b) tangential and (c) radial section with their zoomed portion (d-f) and the optical histology obtained by mechanical cut of (g) transverse, (h) tangential and (i) radial thin section.

3.4. *Entandrophragma cylindricum*

The complete virtual histology of *Entandrophragma cylindricum* (sapele mahogany) obtained by MRI is shown in Fig. 4, together with the conventional optical histology. In the transverse section, this type of wood is characterized by a diffuse porosity with very large vessels (light blue arrows in Fig. 4d and g), many of which are often full of gums or other deposits (pink arrow). The presence of gums is identified by MRI thanks to their characteristic black image voxels. Indeed, the gum is a semi-solid with hydrogens that are characterized by a fast relaxation rate (very short T_2). The growth ring boundary is indistinct in our sample. White arrows in both MR and optical images (Fig. 4d and g) indicate paratracheal parenchyma (parenchyma surrounding vases), which can be described as vasicentric, aliform and confluent. Each

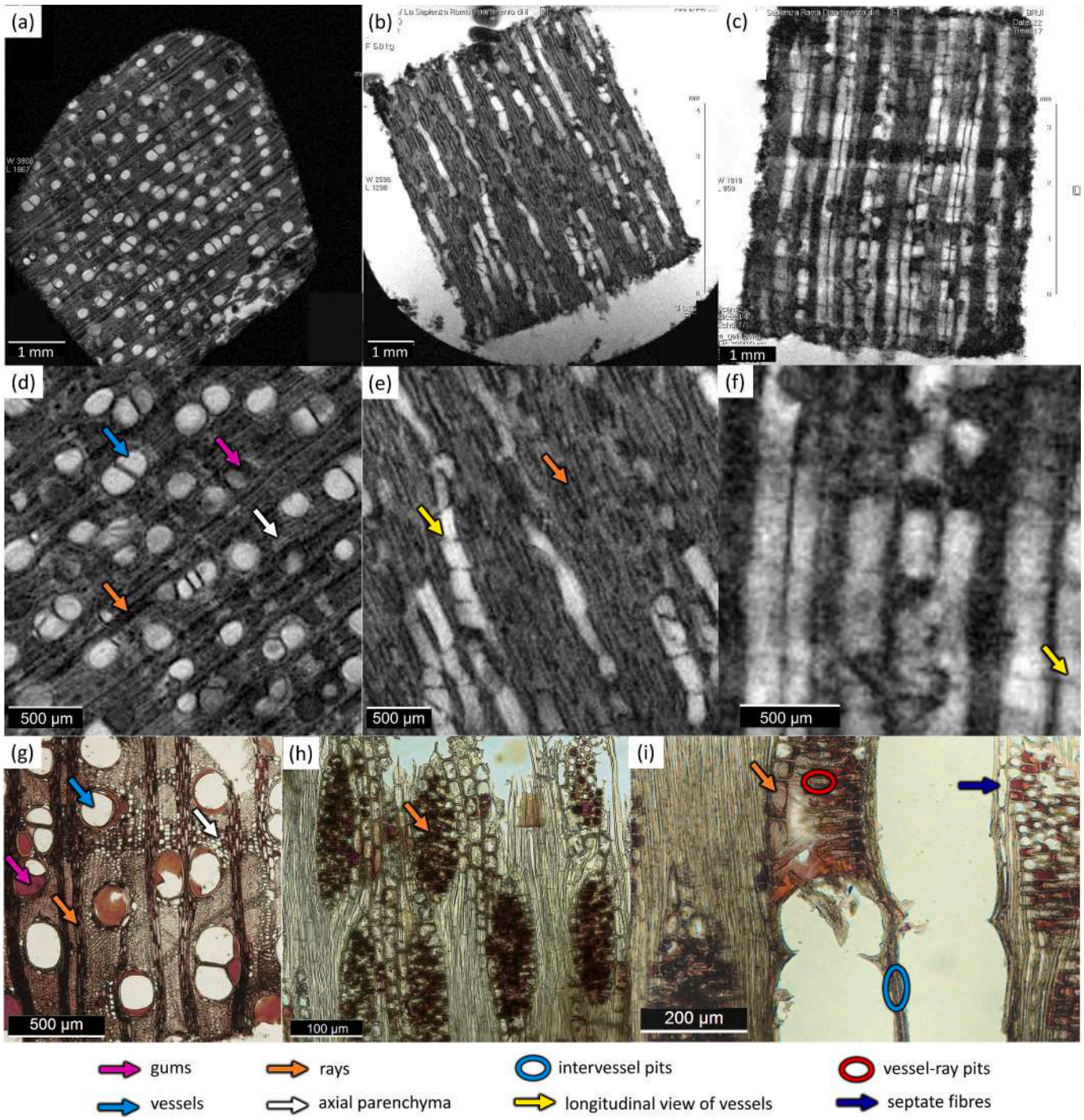

Fig. 4. Diagnostic features of *Entandrophragma cylindricum* (sapele mahogany) wood investigated by the NMR virtual histology of (a) transverse, (b) tangential and (c) radial section with their zoomed portion (d-f) and the optical histology obtained by mechanical cut of (g) transverse, (h) tangential and (i) radial thin section.

parenchyma strand has a width between four and eight cells. The MR images are T_2*-weighted and vessels (5–20 vessels per square millimeter) are identified by bright image voxels because in they contain water with higher mobility and longer T_2 compared to water in parenchyma and other wood structures. Oppositely, parenchyma cells are characterized by darker image voxels due to their smaller lumen size which causes a fast T_2 relaxation. Rays (orange arrows) are highlighted by very dark image voxels due to both the presence of gum deposits and the very small lumen size of their cells. All these factors contribute to an accelerated relaxation of the water quantified with a short T_2.

In the tangential section obtained by MRI (Fig. 4b and e), it is possible to observe the height of rays (orange arrow) and the longitudinal view of vessels (yellow arrow). The rays' height is better visible in the optical microscopy image (Fig. 4h, orange arrow) along with their width, which varies from 4 to 10 cells. It should be noticed that rays are characterized by image voxels similar to those of the fibres in Fig. 4e. This result suggests that rays contain water with a T_2 close to that of fibres, which causes a sharp decrease in the NMR signal intensity at TE = 4 ms. This can be ascribable to the comparable size of cells in rays and fibres or/and to the fact that impurities (gums) in rays may have shortened the T_2 relaxation.

Lastly, the radial section is shown in Fig. 4c, f and i. Although not

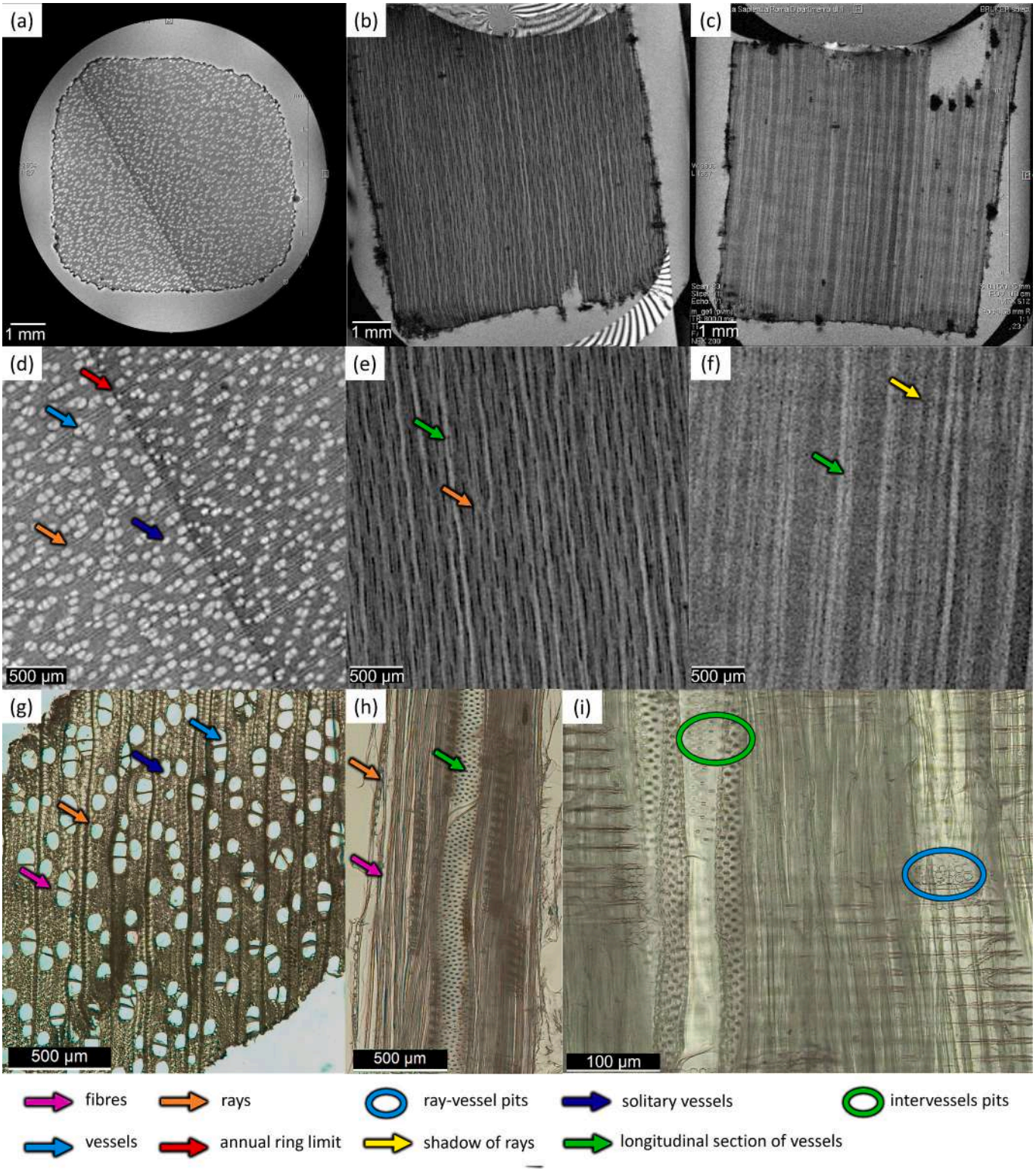

Fig. 5. Diagnostic features of *Populus alba* (white poplar) wood investigated by the NMR virtual histology of (a) transverse, (b) tangential and (c) radial section with their zoomed portion (d-f) and the optical histology obtained by mechanical cut of (g) transverse, (h) tangential and (i) radial thin section.

crucial for the identification of this specific taxon, the anatomical characters can be only detected by optical microscopy. Here, the orange arrow points out the upright ray cells. Rays can be described as heterogeneous, being composed of both elongated and upright cells. Septate (blue arrow) fibres, which are thin- to thick-walled, are present.

3.5. *Populus alba*

MR images in Figures 5 show the anatomy of *Populus alba* (white poplar), a hardwood characterized by diffuse porosity [38]. An annual ring limit is visible in the MR image (Fig. 5d, red arrow). In the optical image, the annual ring limit is not observed (Fig. 5g). This sample of

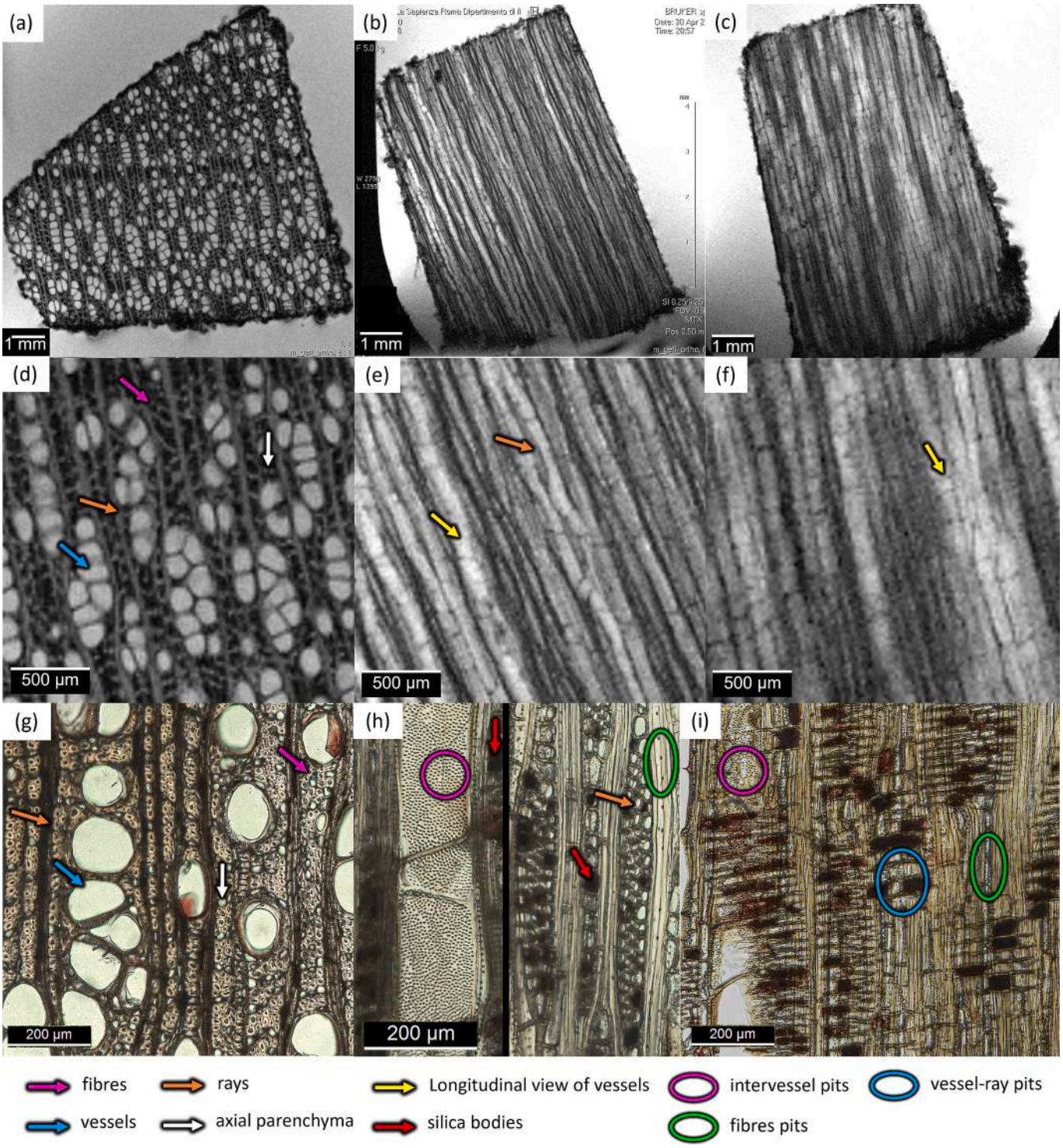

Fig. 6. Diagnostic features of *Pouteria altissima* (tanganyika walnut) wood investigated by the NMR virtual histology of (a) transverse, (b) tangential and (c) radial section with their zoomed portion (d-f) and the optical histology obtained by mechanical cut of (g) transverse, (h) tangential and (i) radial thin section.

wood has vessels homogeneous in size, solitary, or arranged in groups or short radial files (light-blue and blue arrows in Fig. 5d and g). The rays were observed both in the optical microscopy and MR image (orange arrows). The T_2-weighted image of Fig. 5d shows the cross-sectional areas of vessels with bright white voxels due to the longer T_2 of water in vessels compared to the shorter T_2 of water in fibres. The fibres can be observed in Fig. 5g (pink arrow).

Fig. 5b, e and h show the tangential section of poplar. It is possible to see uniseriate rays (orange arrow) and the longitudinal section of vessels (green arrow) in both the MR and optical microscopy image. Fibres can also be observed in Fig. 5h (pink arrow). The optical microscopy image allows us to assess the height of rays as being of 10–15 cells.

In the MR image of the radial section in Fig. 5f we can only see darker streaks in correspondence of rays (yellow arrow) and the longitudinal section of vessels (green arrow). Thanks to the higher resolution reached by optical microscopy, further information can be obtained. We can see the presence of homogeneous rays. Ray-vessels pits are large and simple (light-blue circle) and inter-vessel pits are large (green circle).

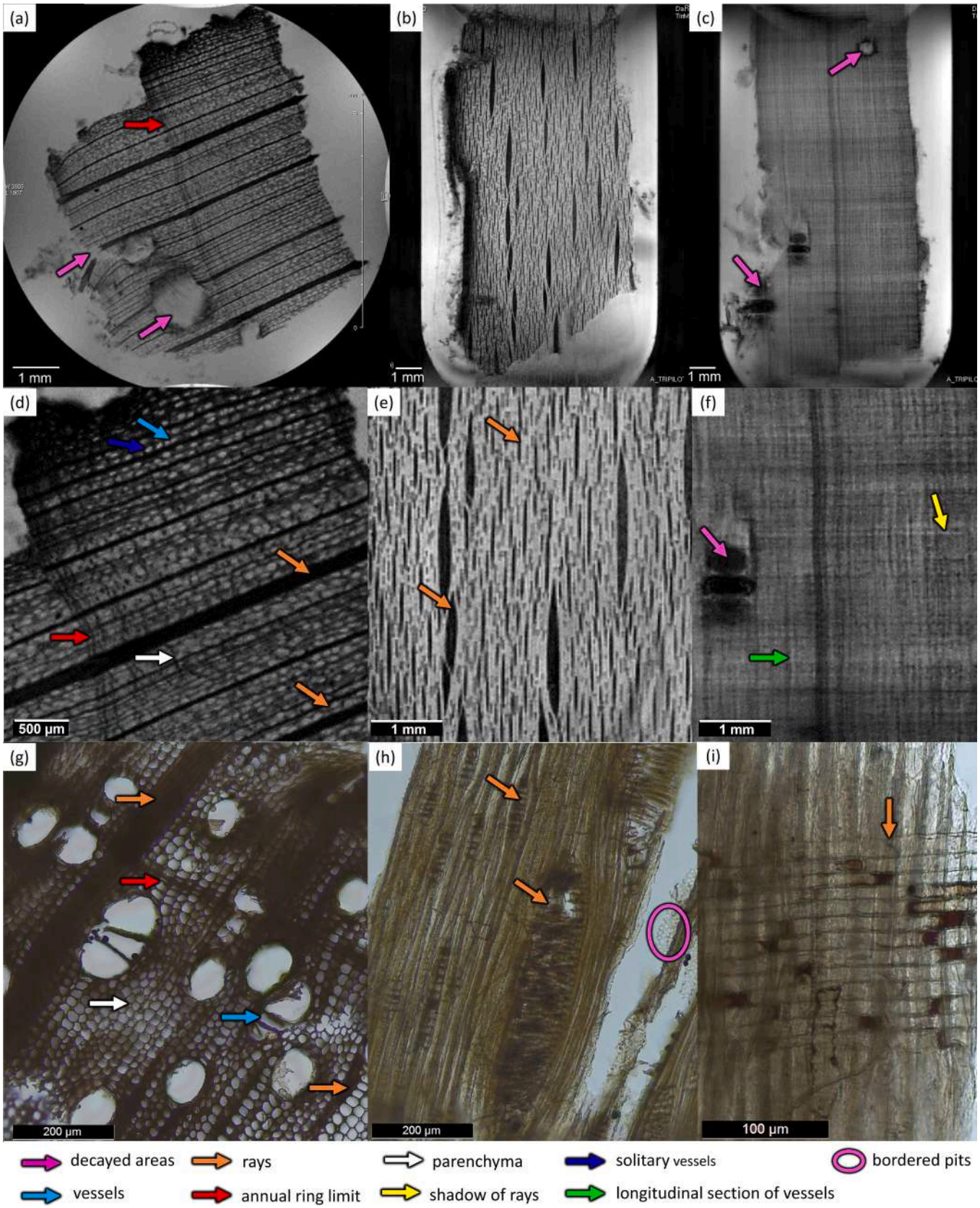

Fig. 7. Diagnostic features of *Fagus sylvatica* (beech tree) wood investigated by the NMR virtual histology of (a) transverse, (b) tangential and (c) radial section with their zoomed portion (d-f) and the optical histology obtained by mechanical cut of (g) transverse, (h) tangential and (i) radial thin section.

3.6. Pouteria altissima

In Fig. 6 the morphology of *Pouteria altissima* (tanganyika walnut) in its three anatomical sections is displayed. The images show that tanganyika walnut has a diffuse porosity. In our sample, ring boundaries are indistinct. In Fig. 6d, a zoomed portion belonging to the MR image of the transverse section is displayed, being comparable to the optical image in Fig. 6g. Here, vessels (5–20 vessels per square millimeter) with a mean diameter of 50–200 μm arranged in radial multiples of 4 (light-blue arrow), along with rays (orange arrow) and thick-walled fibres (pink arrow) can be identified. Moreover, axial parenchyma in narrow bands (white arrow) is visible. Similarly to African walnut (see Fig. 3), fibres lumen is smaller than that of parenchyma cells, as suggested by their different MRI contrast. Ray parenchyma provides bright image voxels which is ascribable to the longer T_2 of water due to larger size of its cells.

The tangential section obtained by MRI (Fig. 6e) allows the observation of rays (orange arrow) and longitudinal section of vessels (yellow arrow). Conversely, the optical image of Fig. 6h shows rays with uniseriate and multiseriate portions, with a width varying between 1 and 4 cells (orange arrow). Fibres have simple to minutely bordered pits (green circle). Silica bodies (red arrows) are present in rays and axial parenchyma cells.

MRI in the radial section (Fig. 6f) allows us to observe vessels (yellow arrow) only longitudinally. Optical microscopy image (Fig. 6i) shows that inter-vessel pits (pink circle) are alternate with small to medium (4–10 μm) size. Vessel-ray pits (light-blue circle) have much reduced borders. Rays are heterogeneous with cells of varying size and shape, such as procumbent, with one row of upright or square marginal cells.

3.7. Archaeological specimen of Fagus cf. sylvatica

In Fig. 7 the anatomy of the archaeological *Fagus* cf. *sylvatica* sample is shown. All the MR images are characterized by a quite dark contrast which suggests the presence of impurities inside the archaeological wood structure. Particularly, all the rays (orange arrows) appear black. This is due to the accumulation of inclusions, as confirmed by both the tangential and radial sections obtained by light microscopy (Fig. 7e and f). The MR images also show many decayed areas (pink arrows) characterized by different contrast. Specifically, areas with light image voxels indicate wood structural damages, such as holes and cavities; areas characterized by dark image voxels correspond to accumulation of decomposed organic material and/or heavy metals; rounded black and large spots indicate bubbles due to the gas emissions of infesting microorganisms (*e.g.,* fungi), as already shown in previous works [2,3,36,40–44].

The transverse section in Fig. 7a allows us to see the annual ring limit (red arrow) and the diffuse-porous ring typical of this wood. Vessels organized in groups of two or three (light-blue arrow) or solitary vessels (blue arrow) are better visible in Fig. 7d and in the optical image of Fig. 7g. Here, an annual ring limit is also visible (red arrow). The white arrows in Fig. 7d and g indicate the apotracheal parenchyma.

The tangential section in Fig. 7e allows to recognize both multiseriate and uniseriate rays (orange arrows) as confirmed by light microscopy in Fig. 7h, where vertical elements such as fibres and vessels can be also seen. Bordered pits along vessels can also be observed (pink circle in Fig. 7h).

In Fig. 7f the radial section images obtained by MRI only shows the shadow of rays (yellow arrow) and the longitudinal section of vessels (green arrow). These diagnostic features were instead well resolved in the light microscopy image of Fig. 7i, where it is possible to see a homogeneous ray (orange arrow) made up of elongated cells. Brown inclusions can also be observed.

3.8. 3D reconstruction of E. cylindricum sample

The 3D reconstruction of the sample volume of *E. cylindricum* (sapele mahogany) is presented in Fig. 8, and three 2D images at different heights in the sample are also shown. The 3D reconstruction provides the overall morphology of the sample volume. It is possible to observe the length of vessels, which run through the entire wood sample. Vessels appear as non-linear (wavy) tubular structures completely full of water characterized by long T_2 value, as suggested by their light image voxels. The sample is also characterized by black areas, located both inside and outside the vessels, which represent the distribution of gums within and along the sample volume.

In Fig. 9a, the rotated 3D reconstruction of *E. cylindricum* sample helps to better recognize some characteristics of this wood species, such as gums deposits (red arrow) and parenchyma cells (green arrow). Fig. 9b shows that by cutting the 3D reconstructed wood it is possible to obtain a tangential section where rays are visible (yellow arrow).

Moreover, in Fig. 8c the histogram of voxels intensity in the grayscale calculated over the 24 2D NMR images is displayed. The plot indicates that in grayscale with 255 tones, where 255 corresponds to white voxels and 0 corresponds to black voxels, most of the voxels are associated with a tone around 65 that corresponds to a dark gray tone, whereas much fewer voxels are light gray. The histogram allows us to quantify, along the entire sample, the number of voxels characterized by different grayscale tones that depend on the different NMR signal intensity, which in turn is affected by the water mobility within the wood structure. In this way, it is possible to have an estimate of how much bound or free water is stored in the sample. Hence, histograms similar to that shown in Fig. 8c could be used to study the water dynamics in different wood types, which is indicative of the different size of their anatomical elements, and how water dynamics change with degradation in archaeological wood samples, as similarly done in previous works [2,40,41] .

3.9. Final remarks

A summary of the diagnostic characters observed in this work by light microscopy and μ-MRI for softwoods and hardwoods is presented, respectively, in Tables 4 and 5. In softwoods, μ-MRI does not allow to see the cell wall thickness in the transverse section. In contrast, all the diagnostic characters of hardwoods can be observed in the transversal view. While MRI allows us to distinguish and characterize vessels and rays in the tangential section, ray cells and bordered pits cannot be seen in both hardwoods and softwoods. Finally, the radial section obtained by MRI does not provide diagnostic information in either case. This result suggests that μ-MRI can provide informative images, by a non-destructive and virtual sectioning of the wood sample, which are able to distinguish between softwoods and hardwoods and a more precise identification can be reached for hardwoods. The advantages and disadvantages at the current state of the two techniques used in this study for the investigation of modern and ancient waterlogged wood are illustrated in Table 6. In this work, μ-MRI attained a maximum in-plane resolution of 8×8 μm^2, which is lower than that of optical microscopy. Nevertheless, the image resolution in MRI is not a physical limit but depends on the magnetic field gradient strength. Spectrometers equipped with stronger magnetic gradients are even able to reach resolutions around 1 μm. At the current state, μ-MRI retains a higher cost and longer experiment time than those required with optical microscopy but μ-MRI is based on the virtual cut of thin slices, therefore avoids sample destruction and/or manipulation, better preserving it for further analyses. This makes it easier to perform on archaeological waterlogged wood and very small samples compared to optical microscopy. μ-MRI also allows the 3D reconstruction of the entire wood sample, which cannot be obtained with light microscopy. The MRI 3D model provides an overall view of the wood volume of interest.

4. Conclusion

In this work the anatomy of six modern waterlogged wood samples and one archaeological waterlogged wood sample belonging to seven

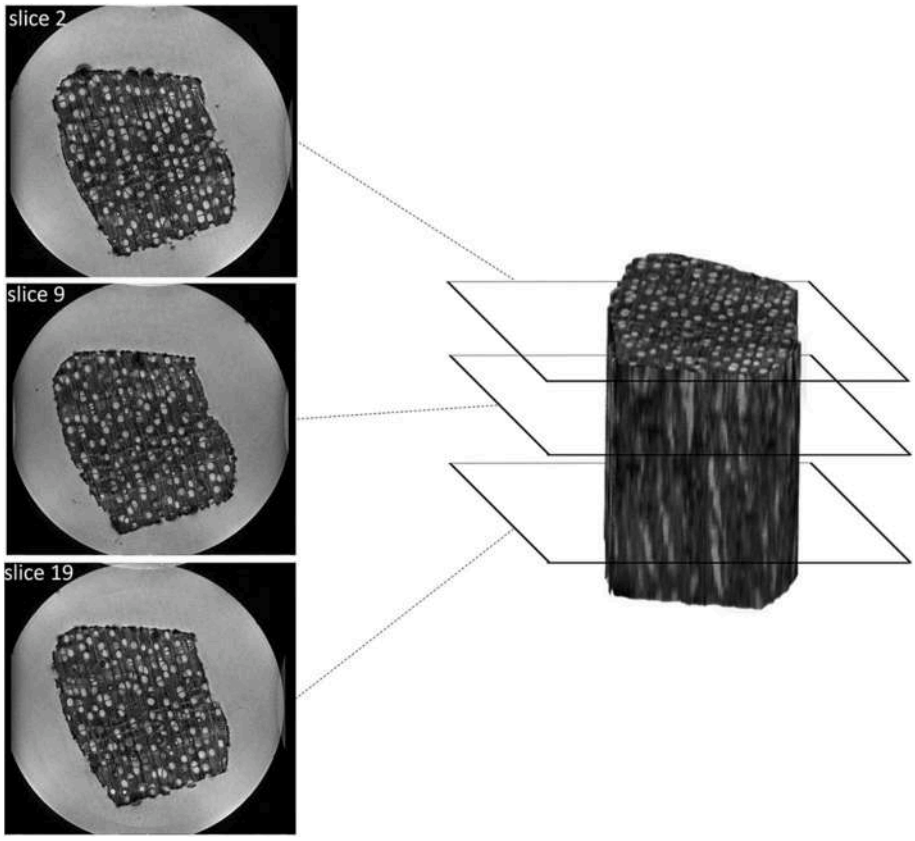

Fig. 8. 3D reconstruction of *E. cylindricum* (sapele mahogany) sample obtained by processing of 2D MR images.

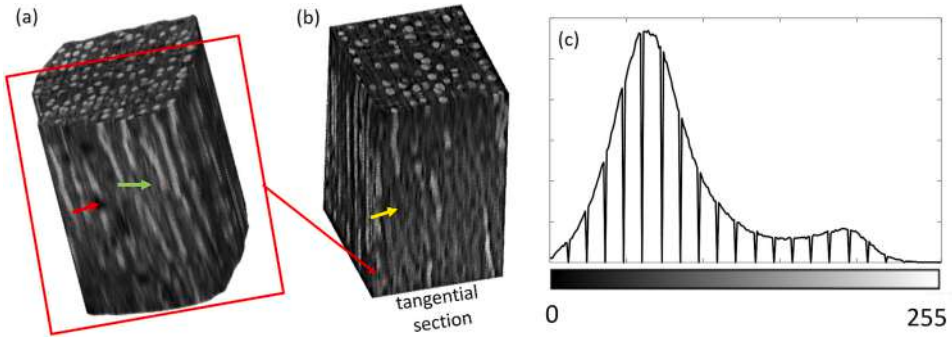

Fig. 9. (a) Rotated 3D reconstruction, (b) tangential cut of 3D reconstruction and (c) histogram of voxels intensity in a grayscale with 255 tones obtained from 2D NMR images of *E. cylindricum* (sapele mahogany). In (a) the red and green arrows represent gums and parenchyma cells; in (b) the yellow arrow indicates the ray. (For interpretation of the references to colour in this figure legend, the reader is referred to the web version of this article.)

Table 4
Diagnostic characters observable by light microscopy and μ-MRI in softwoods.

Softwoods	Light microscopy	μ-MRI
Trasverse section		
Annual ring limits	X	X
Resin canals	X	X
Cell wall thickness	X	–
Rays	X	X
Tangential section		
Rays	X	X
Resin canals	X	X
Ray cells (ray height)	X	–
Bordered pits	X	–
Radial section		
Pits in cross-fields	X	–

Table 5
Diagnostic characters observable by light microscopy and μ-MRI in hardwoods.

Hardwoods	Light microscopy	μ-MRI
Trasverse section		
Annual ring limits	X	X
Porosity (diffuse, ring-porous)	X	X
Axial parenchyma	X	X
Gums and other deposits	X	X
Tangential section		
Rays	X	X
Vessels	X	X
Ray cells (thickness and height of rays)	X	–
Radial section		
Inter-vessel pits	X	–
Vessel-ray pits	X	–
Homogeneous/heterogenous rays	X	–

Table 6
Advantages and disadvantages of light microscopy and μ-MRI used in this work.

	Advantages	Disadvantages
Light microscopy	• Images with higher resolution • Observation of all diagnostic characters • Identification of decay type • Lower cost • Shorter experiment time	• (Micro)destructive • No 3D-recostruction • Difficult to perform on archaeological waterlogged wood or extremely small wood samples • Number of images from one sample depending on the number of thin sections
μ-MRI	• Non-destructive • Analysis of the whole sample volume by 3D reconstruction • Easy to perform on archaeological waterlogged wood and extremely small wood samples • Infinite number of images from one sample • Identification of decay type and its distribution along all the sample volume	• Still insufficient resolution of images in longitudinal sections • Not applicable for the identification of all wood species • Higher cost • Longer experiment time

different species was studied by a non-conventional methodology, *i.e.,* micro-Magnetic Resonance Imaging (μ-MRI) with a maximum in-plane resolution of 8×8 μm^2. To the best of our knowledge, this is the first study in which μ-MRI is used to provide high-resolution images of the three anatomical sections of wood and compared with light microscopy. The results discussed in this work suggest that traditional optical microscopy remains superior to μ-MRI in the species identification, due to the higher resolution that it attains. Small wood samples (with diameter smaller than 1 cm) were studied in this work. This restriction on the sample size, as well as the MR image resolution reached in this work, is not an intrinsic limit of μ-MRI technique but it depends on the NMR spectrometer used (*i.e.,* size of the access bore). In conclusion, this work shows that multi-parametric μ-MRI combined with light microscopy is able to achieve a better understanding of waterlogged archaeological wood samples, such as their conservation state and the possible causes of all their alterations. The present work represents a starting point for further improvements of μ-MRI techniques for the non-destructive investigation of waterlogged wood samples, especially those of interest for cultural heritage. We hope that the technological development of NMR scanners will also consider this new field of application: the non-destructive study of waterlogged wood.

Author contributions

***VS*, CM and SC:** Conceptualization; ***VS* and CM:** Data curation; ***VS* and CM:** Formal analysis; **LS and SC:** Funding acquisition; ***VS*, CM and SC:** Investigation; ***VS*, CM and SC:** Methodology; **LS and SC:** Project administration; **LS, SC, ED and RR:** Resources; ***VS* and CM:** Software; **LS and SC:** Supervision; ***VS*, CM, LS, ED, RR and SC:** Validation; ***VS*, CM and SC:** Visualization; ***VS* and CM:** Roles/Writing - original draft; ***VS*, CM and SC:** Writing - review & editing.

Acknowledgments

The authors would like to thank Dr. Mario Mineo of Museum of Civilizations of Rome for providing the archaeological wooden specimen.

References

[1] Hickey M, King C. The Cambridge illustrated glossary of botanical terms. 1st ed. Cambridge: Cambridge University Press; 2001.
[2] Stagno V, Capuani S. Decay of a Roman age pine wood studied by micro magnetic resonance imaging , diffusion nuclear magnetic resonance and portable nuclear magnetic resonance. Acta IMEKO 2022;11:1–10. https://doi.org/10.21014/acta_imeko.v11i1.1079.
[3] Capuani S, Stagno V, Missori M, Sadori L, Longo S. High-resolution multiparametric MRI of contemporary and waterlogged archaeological wood. Magn Reson Chem 2020;58:860–9. https://doi.org/10.1002/mrc.5034.
[4] Ruffinatto F, Cremonini C, Macchioni N, Zanuttini R. Application of reflected light microscopy for non-invasive wood identification of marquetry furniture and small wood carvings. J Cult Herit 2014;15:614–20. https://doi.org/10.1016/j.culher.2013.11.013.
[5] High KE, Penkman KEH. A review of analytical methods for assessing preservation in waterlogged archaeological wood and their application in practice. Herit Sci 2020;8:83. https://doi.org/10.1186/s40494-020-00422-y.
[6] Longo S, Mormina E, Granata F, Mallamace D, Longo M, Capuani S. Investigation of an Egyptian mummy board by using clinical multi-slice computed tomography. Stud Conserv 2018;63:383–90. https://doi.org/10.1080/00393630.2018.1439805.
[7] Ghavidel A, Hofmann T, Bak M, Sandu I, Vasilache V. Comparative archaeometric characterization of recent and historical oak (Quercus spp.) wood. Wood Sci Technol 2020;54:1121–37. https://doi.org/10.1007/s00226-020-01202-4.
[8] Moricca C, Nigro L, Masci L, Pasta S, Cappella F, Spagnoli F, et al. Cultural landscape and plant use at the Phoenician site of Motya (Western Sicily, Italy) inferred from a disposal pit. Veg Hist Archaeobotany 2021;30:815–29. https://doi.org/10.1007/s00334-021-00834-1.
[9] Silva JL, Barata CS, Pissarra J. Limitations and obstacles on wood identification from sculptures - analysis of a set of gilded and polychromed Flemish artworks from the 15th century. Int J Conserv Sci 2021;12:349–60.
[10] Comparative Carlquist S, Anatomy Wood. Systematic, ecological, and evolutionary aspects of Dicotyledon wood. 2nd ed. Berlin, Heidelberg: Springer; 2001.
[11] Abe H. Wood Identification Research and Its Importance. Mokuzai Gakkaishi; 2016. https://doi.org/10.2488/jwrs.62.240.
[12] Wheeler EA, Baas P. Wood identification - a review. IAWA J 1998. https://doi.org/10.1163/22941932-90001528.
[13] Bruzzone R, Galassi MC. Wood species in Italian panel paintings of the fifteenth and sixteenth centuries: historical investigation and microscopical wood identification. Stud old master Paint Technol Pract Natl Gall Tech Bull 30th Anniv. Conf. postprints. 2011. p. 253–9.
[14] Svedström K, Bjurhager I, Kallonen A, Peura M, Serimaa R. Structure of oak wood from the Swedish warship Vasa revealed by X-ray scattering and microtomography. Holzforschung 2012;66:355–63. https://doi.org/10.1515/hf.2011.157.
[15] Mouzouras R, Jones AM, Jones EBG, Rule MH. Non-destructive evaluation of hull and stored timbers from the Tudor ship Mary Rose. Stud Conserv 1990;35:173–88. https://doi.org/10.1179/sic.1990.35.4.173.
[16] Ruffinatto F, Macchioni N, Boetto G, Baas P, Zanuttini R. Reflected light microscopy as a non-invasive identification tool for wooden artefacts. IAWA J 2010;31:317–31. https://doi.org/10.1163/22941932-90000026.
[17] Čufar K, Balzano A, Krže L, Merela M. Wood identification using non-destructive confocal laser scanning microscopy. Les/Wood 2019;68:19–29. https://doi.org/10.26614/les-wood.2019.v68n02a02.
[18] Cai C, Javed MA, Komulainen S, Telkki VV, Haapala A, Heräjärvi H. Effect of natural weathering on water absorption and pore size distribution in thermally modified wood determined by nuclear magnetic resonance. Cellulose 2020;27:4235–47. https://doi.org/10.1007/s10570-020-03093-x.
[19] Kanazawa Y, Yamada T, Kido A, Fujimoto K, Takakura K, Hayashi H, et al. Internal evaluation of impregnation treatment of waterlogged wood; relation between concentration of internal materials and relaxation time using magnetic resonance imaging. Magn Reson Imaging 2017;38:196–201. https://doi.org/10.1016/j.mri.2017.01.010.
[20] Stelzner J, Stelzner I, Martinez-Garcia J, Gwerder D, Wittköpper M, Muskalla W, et al. Stabilisation of waterlogged archaeological wood: the application of structured-light 3D scanning and micro computed tomography for analysing dimensional changes. Herit Sci 2022;10:60. https://doi.org/10.1186/s40494-022-00686-6.
[21] Van Den Bulcke J, Boone M, Van Acker J, Stevens M, Van Hoorebeke L. X-ray tomography as a tool for detailed anatomical analysis. Ann For Sci 2009;66:508. https://doi.org/10.1051/forest/2009033.
[22] Telkki VV. Wood characterization by NMR & MRI of fluids. eMagRes 2012. https://doi.org/10.1002/9780470034590.emrstm1298.
[23] Brodersen CR. Visualizing wood anatomy in three dimensions with high-resolution X-ray micro-tomography (MCT) - a review. IAWA J 2013. https://doi.org/10.1163/22941932-00000033.
[24] Re A, Albertin F, Avataneo C, Brancaccio R, Corsi J, Cotto G, et al. X-ray tomography of large wooden artworks: the case study of “Doppio corpo” by Pietro Piffetti. Herit Sci 2014;2:1–9. https://doi.org/10.1186/s40494-014-0019-9.
[25] Sedighi Moghaddam M, Van Den Bulcke J, Wålinder MEP, Claesson PM, Van Acker J, Swerin A. Microstructure of chemically modified wood using X-ray

computed tomography in relation to wetting properties. Holzforschung 2017;71:119–28. https://doi.org/10.1515/hf-2015-0227.
[26] Brodersen CR, Roddy AB. New frontiers in the three-dimensional visualization of plant structure and function. Am J Bot 2016;103:184–8. https://doi.org/10.3732/ajb.1500532.
[27] Mori M, Kuhara S, Kobayashi K, Suzuki S, Yamada M, Senoo A. Non-destructive tree-ring measurements using a clinical 3T-MRI for archaeology. Dendrochronologia 2019;57:125630. https://doi.org/10.1016/j.dendro.2019.125630.
[28] Stagno V, Egizi F, Corticelli F, Morandi V, Valle F, Costantini G, et al. Microstructural features assessment of different waterlogged wood species by NMR diffusion validated with complementary techniques. Magn Reson Imaging 2021;83:139–51. https://doi.org/10.1016/j.mri.2021.08.010.
[29] Slichter CP, Hahn EL. Principles of magnetic resonance. 2nd ed. 1979. https://doi.org/10.1063/1.2995411. Phys Today.
[30] Callaghan PT. Principle of nuclear magnetic resonance microscopy. 1994.
[31] Farrar TC, Becker ED. Pulse and Fourier transform NMR. 1st ed. New York and London: Academic Press; 1971. https://doi.org/10.1016/b978-0-08-091812-9.50001-6.
[32] Stagno V, Ricci S, Longo S, Verticchio E, Frasca F, Maria A, et al. Discrimination between softwood and hardwood based on hemicellulose content obtained with portable nuclear magnetic resonance. Cellulose 2022;29:7917–34. https://doi.org/10.1007/s10570-022-04728-x.
[33] Jezzard P, Clare S. Principles of nuclear magnetic resonance and MRI. 2012. https://doi.org/10.1093/acprof:oso/9780192630711.003.0003.
[34] Schulz H, Postma JA, Van Dusschoten D, Scharr H, Behnke S. 3D reconstruction of plant roots from MRI images. VISAPP 2012 - Proc. Int Conf Comput Vis Theory Appl. 2012. p. 24–33. https://doi.org/10.5220/0003869800240033.
[35] Mori M, Kuhara S, Kobayashi K, Suzuki S. Nondestructive visualization of polyethylene glycol impregnation in wood using ultrashort echo time 3D imaging. J Cult Herit 2021;50:43–8. https://doi.org/10.1016/j.culher.2021.05.008.
[36] Beccaccioli M, Moricca C, Faino L, Reale R, Mineo M, Reverberi M. The Neolithic site "La Marmotta": DNA metabarcoding to identify the microbial deterioration of waterlogged archeological wood. Front Microbiol 2023;14:1129983. https://doi.org/10.3389/fmicb.2023.1129983.
[37] WFO. World Flora Online 2023:2023. http://www.worldfloraonline.org/taxon/wfo-0000498648 (accessed January 25, 2023).
[38] Schweingruber FH, Anatomy of European Woods. An Atlas for the identification of European Trees. Shrubs and Dwarf Shrubs. Verlag Paul Haupt.; 1990. ISBN 9783258042589.
[39] Wheeler EA. InsideWood - a web resource for hardwood anatomy. IAWA J 2011. https://doi.org/10.1163/22941932-90000051.
[40] Stagno V, Longo S, Capuani S. Effect of age on Pine wood microstructure studied by micro-MRI and diffusion-NMR. 2020 IMEKO TC-4 Int. Conf. Metrol. Archaeol. Cult. Herit. 2020.
[41] Stagno V, Mailhiot S, Capuani S, Galotta G, Telkki VV. Testing 1D and 2D single-sided NMR on Roman age waterlogged woods. J Cult Herit 2021;50:95–105. https://doi.org/10.1016/j.culher.2021.06.001.
[42] Cole Hamilton D, Kaye B, Chudek JA, Hunter G. Nuclear magnetic resonance imaging of waterlogged wood. Stud Conserv 1995;40:41–50. https://doi.org/10.1179/sic.1995.40.1.41.
[43] Cole-Hamilton DJ, Chudek JA, Hunter G, Martin CJM. N.M.R. imaging of water in wood including water-logged archaeological artefacts. J Inst Wood Sci 1990;12:111–3.
[44] Longo S, Egizi F, Stagno V, Di Trani MG, Marchelletta G, Gili T, et al. A multi-parametric investigation on waterlogged wood using a magnetic resonance imaging clinical scanner. Forests 2023;14:276. https://doi.org/10.3390/f14020276.